ON THE SOLUTION OF THE UNSTEADY NAVIER-STOKES EQUATIONS FOR HYPERSONIC FLOW ABOUT AXIALLY-SYMMETRIC BLUNT BODIES

eirs

ENGINEERING & INDUSTRIAL RESEARCH STATION

Aerospace Engineering

By

Z. U. A. Warsi

R. A. Weed

J. F. Thompson

Prepared by

Mississippi State University
Engineering and Industrial Research Station
Department of Aerospace Engineering
Mississippi State, Ms. 39762

Mississippi State University
Mississippi State, Ms. 39762

MSSU-EIRS-ASE-6

On the Solution of the Unsteady Navier-Stokes Equations for Hypersonic Flow About Axially-Symmetric Blunt Bodies

by

Z. U. A. Warsi, R. A. Weed and J. F. Thompson

Report Number MSSU-EIRS-ASE-80-6

Prepared by

Mississippi State University
Engineering and Industrial Research Station
Department of Aerospace Engineering
Mississippi State, MS 39762

Final Technical Report
For the Period, May 1978-September 1980
Prepared for George C. Marshall Space Flight Center
Marshall Space Flight Center, Alabama 35812
Under Contract NAS8-32912
September 1980

ABSTRACT

Hypersonic flow about a body of revolution with or without an angle of attack is of much interest both from the design and computational view points. In this paper a formulation of the complete Navier-Stokes problem for a viscous hypersonic flow in general curvilinear coordinates is presented. This formulation is applicable to both the axially symmetric and three-dimensional flows past bodies of revolution. The equations for the case of zero angle of attack have been solved past a circular cylinder with hemispherical caps by point SOR finite difference approximation. The free stream Mach number and the Reynolds number for the test case are respectively 22.04 and 168888. The whole algorithm is presented in detail along with the preliminary results for pressure, temperature, density and velocity distributions along the stagnation line.

1. INTRODUCTION

The problem of predicting the flowfield about arbitrary blunt bodies traveling at supersonic and hypersonic speeds has been the subject of much theoretical and experimental research. Supersonic flow about blunt bodies is characterized by a detached bow shock wave around the nose of the body that divides the flowfield into regions of supersonic and subsonic flow. The existence of these regions of mixed flow has limited existing analytical methods for the blunt body problem to semiempirical techniques or inviscid flow approximations. However, these methods cannot simultaneously predict flow properties in all regions of the flowfield. In addition, the relationship between the shape of the body and the shape and location of the bow shock has restricted most existing solutions to relatively simple body shapes.

In an effort to overcome the problems associated with existing approximate methods, several researchers have developed numerical solutions of the full set of governing equations for fully compressible, viscous flow, viz., the Navier-Stokes equations, by finite difference techniques. Unfortunately, the problems inherent in numerical solution of the Navier-Stokes equations have usually outweighed the techniques' usefulness as a research tool. In particular, the numerical instabilities that arise from replacing the actual equations with finite difference approximations and the large computational fields required for accurate resolution of the flowfield have, in the past, prevented the treatment of problems of practical interest, i.e., arbitrary body shapes and high Reynolds Number flows. However, in recent years, the continuing improvement of digital computers and the introduction of more efficient numerical methods have made treatment of realistic problems feasible.

The present investigation presents a method for the numerical solution of the Navier-Stokes equations for both supersonic and hypersonic viscous flow about arbitrarily shaped blunt bodies.

The techniques used in this research are an extension of the methods introduced by Warsi, Devarayalu, and Thompson [1,2] and Devarayalu [3] for supersonic flow about 2D blunt bodies. The Navier-Stokes equations are first transformed from Cartesian coordinates to a set of general coordinates by applying basic relations from tensor analysis. The numerical techniques developed by Thompson, Thames, and Mastin [4,5,6] are then used to generate a boundary fitted curvilinear coordinate system for prescribed body and outer boundary shapes. This type of coordinate system will map into a rectangular coordinate grid in the transformed plane. Since the body and the outer boundary become straight lines in the transformed plane, the statement of boundary conditions for arbitrary body shapes is greatly simplified. In addition, this method of generating coordinates allows coordinate lines to be concentrated in any region in the field. A dense mesh system can then be imposed in regions of large gradients in the flow variables such as boundary layers or across shock waves.

In the current investigation, a new approach to the transformation of the Navier-Stokes equations has been employed. Warsi [7] has shown that the transformed equations can be written in a form that retains the conservation law or "divergence" form of the original equations for all cases except axisymmetric flow. Conservation equations are favored in compressible flow problems because they will satisfy the Rankine-Hugoniot relations for shock waves when the differencing scheme applied to the equations is conservative.

The next step in the solution process is the development of an algorithm to solve the transformed equations numerically. In this

research, the solution of the transformed equations was accomplished by replacing the partial derivatives in the equations with finite difference approximations that produce a set of implicit finite difference equations. These equations are then solved by the Successive Over Relaxation (SOR) iterative technique. The implicit formulation was chosen for its unconditional stability. The conservation law form of the equations allows construction of simple, easily programmed S.O.R. algorithms.

In the present investigation, the Navier-Stokes equations were solved at all points in the field. The bow shock appears in the field as a zone of transition of the flow variable smeared over a few grid lines. This technique is called "shock capturing." However, several authors [8,9,10] have found this technique to be impractical for large Reynolds Number flows because of the numerical difficulties associated with the large gradients that appear in the flow variables in the regions where the bow shock forms. Instead, they treat the shock as a boundary across which the Rankine-Hugoniot equations are applied. The Navier-Stokes equations are solved only in the region behind the bow shock. The flow in front of the shock is considered inviscid. This technique is called "shock fitting." While generally favored, implementation of the "shock fitting" technique can be quite complicated for arbitrary body shapes. Therefore, in spite of the numerical difficulties associated with shock-capturing, this technique was used in the present research because of its simplicity.

Numerical solutions of the Navier-Stokes equations by finite difference techniques are plagued by various types of numerical instabilities. These instabilities appear as oscillations in the flow variables that, if left unchecked, will cause the solution to diverge. These oscillations can be controlled by introducing dissipation into

the solution by either dissipative differencing schemes or explicit artificial viscosity terms added to the calculation of the viscosity coefficient. Both of these methods were used in the present research.

All of the techniques described in this section were used to develop a computer program [11] to solve the Navier-Stokes equations for the case of axisymmetric flow of a perfect gas about a blunt body traveling at hypersonic speed. The axisymmetric flow case was chosen in order to provide initial data for an eventual extension of the program to 3D flow. The body used in this research consists of a circular cylinder with two hemispherical caps. The freestream Mach Number is 22.04. The Reynolds Number based on body diameter is 168888, and the Knudsen number for this flow is about .0002.

2. FORMULATION OF THE PROBLEM

For the purpose of solving the blunt body problem in general body oriented curvilinear coordinate systems, we consider the non-dimensional Navier-Stokes equations in the invariant tensor form. The formulation presented here is for a real gas which is assumed to be thermally though not necessarily calorically perfect. A computer program based on these general considerations has been developed which can also be easily used for calorically perfect gases.

A dimensional quantity is denoted by a superscript * and the value of a quantity at free stream by a subscript ∞. The equations have been non-dimensionalized by using the following free stream values.

L^*	for all lengths
U_∞^*	for velocity vector
ρ_∞^*	density
$\rho_\infty^* U_\infty^{*2}$	for pressure and energy per unit volume
T_∞^*	temperature
μ_∞^*	viscosity
$C_{p^\infty}^*$	specific heat at constant pressure

The non-dimensional form of the conservation equations are

$$\frac{\partial \rho}{\partial t} + \text{div}(\rho \underset{\sim}{v}) = 0 \tag{2.1}$$

$$\frac{\partial}{\partial t}(\rho \underset{\sim}{v}) + \text{div}\ \tilde{\tau} = 0 \tag{2.2}$$

$$\frac{\partial \Psi}{\partial t} + \text{div}\ \underset{\sim}{b} = 0 \tag{2.3}$$

where

$$\tilde{\tau} = \rho \underset{\sim}{v}\underset{\sim}{v} + p\tilde{I} - \varepsilon\tilde{\sigma}$$

$$\tilde{\sigma} = K\tilde{I} + \tilde{d}$$

$$K = \lambda \operatorname{div} \underset{\sim}{v}$$

$$\tilde{d} = \mu \operatorname{def} \underset{\sim}{v}$$

$$\underset{\sim}{b} = (\Psi + p)\underset{\sim}{v} - \varepsilon\tilde{\sigma}\cdot\underset{\sim}{v} - S\mu \operatorname{grad} T \qquad (2.4)$$

$$\Psi = \rho e + \frac{1}{2}\rho|\underset{\sim}{v}|^2$$

$$\varepsilon = 1/R_e = \mu_\infty^*/\rho_\infty^* U_\infty^* L^*$$

$$S = \varepsilon T_\infty^* C_{p\infty}^* C_p / P_r U_\infty^{*2}$$

$$P_r = \mu^* C_p^*/k^*$$

k^* = dimensional fluid conductivity.

In Eqs. (2.4), μ and λ are the non-dimensional first and second coefficients of viscosity respectively.

The set of equations (2.1) - (2.4) form a closed system when the following additional conditions are associated with them.

(i) The equation of state

$$p = C_1(\gamma - 1)\rho T C_p/\gamma \qquad (2.5)$$

where

$$C_1 = C_{p\infty}^* T_\infty^*/U_\infty^{*2}$$

C_p = non-dimensional specific heat at constant pressure

γ = ratio of specific heats .

Both C_p and γ are assumed to be functions of temperature T.

(ii) Sutherland's viscosity law:

$$\mu = (1 + S_1)T^{3/2}/(T + S_1) \tag{2.6}$$

where $S_1 = D^*/T_\infty^*$, $D^* = 110.33^\circ K$.

(iii) Stokes' law:

$$3\lambda + 2\mu = 0 . \tag{2.7}$$

(iv) Eucken's formula:

$$P_r(T) = 4\gamma/(9\gamma - 5) \tag{2.8}$$

The temperature T is obtained by solving a fifth degree equation defined as, (see appendix).

$$(A_1 - 1)T + \tfrac{1}{2}(A_2T_\infty^*)T^2 + \tfrac{1}{3}(A_3T_\infty^{*2})T^3$$

$$+ \tfrac{1}{4}(A_4T_\infty^{*3})T^4 + \tfrac{1}{5}(A_5T^{*4})T^5$$

$$= \frac{1}{C_2}\left(\frac{\Psi}{\rho} - \tfrac{1}{2}|\underset{\sim}{v}|^2\right) \tag{2.9}$$

where

$$C_2 = C_1/f(1)$$

$$f(T) = A_1 + (A_2T_\infty^*)T + (A_3T_\infty^{*2})T^2$$

$$+ (A_4T_\infty^{*3})T^3 + (A_5T_\infty^{*4})T^4 \tag{2.10}$$

The constants A_i are

$$A_1 = 3.6535$$

$$A_2 = -1.33736 \times 10^{-3}/^{o}K$$

$$A_3 = 3.29421 \times 10^{-6}/(^{o}K)^2$$

$$A_4 = -1.91142 \times 10^{-9}/(^{o}K)^3$$

$$A_5 = 0.275462 \times 10^{-12}/(^{o}K)^4$$

On transformation, Eqs. (2.1) - (2.3) have been expressed in the strong conservation-law form (cf. Warsi [7]) as follows

$$\frac{\partial \sigma}{\partial t} + \frac{\partial}{\partial \xi^i}(\sigma v^i) = 0 \tag{2.11}$$

$$\frac{\partial}{\partial t}(\sigma \underset{\sim}{v}) + \frac{\partial}{\partial \xi^k}(X^{ik} \underset{\sim}{a}_i) = 0 \tag{2.12}$$

$$\frac{\partial E}{\partial t} + \frac{\partial Y^i}{\partial \xi^i} = 0 \tag{2.13}$$

Where ξ^i $(i = 1,2,3)$ are the curvilinear coordinates, v^i are the contravariant components of the velocity vector $\underset{\sim}{v}$, and $\underset{\sim}{a}_i$ are the covariant base vectors. Further,

$$\sigma = \sqrt{g}\,\rho$$

$$X^{ik} = \sigma v^i v^k + g^{ik}(P - \varepsilon\chi) - \varepsilon D^{ik}$$

$$Y^i = (E + P)v^i - \varepsilon\psi^i - S\mu\sqrt{g}\, g^{ij} \frac{\partial T}{\partial \xi^j}$$

$$P = \sqrt{g}\, p \ , \ E = \sqrt{g}\, \Psi \ , \ \chi = \sqrt{g}\, K$$

$$\psi^i = \sqrt{g}[Kv^i + \mu(g^{ik}g_{jm}v^j_{,k} + v^i_{,m})v^m \tag{2.14}$$

$$D^{ij} = \sqrt{g}\, d^{ij}$$

and g is the determinant of the coefficient matrix g_{ij}.

2.1 Axially-Symmetric Body

We now particularize the equations for the case of flow past an axially symmetric body of arbitrary shape. Referring to Fig. 1 let $\xi^1 = \xi$, $\xi^2 = \eta$ be the coordinates in the meridian plane and $\xi^3 = \phi$ the azimuthal angle, where x is the axis of symmetry. Thus the generation of the coordinates ξ and η, with η = constant along the body contour, is exactly a two-dimensional problem. The forms of g_{ij}, g^{ij}, and Γ^i_{jk} (the Christoffel symbols) for the axially symmetric body are:

$$g_{11} = x_\xi^2 + r_\xi^2$$

$$g_{22} = x_\eta^2 + r_\eta^2$$

$$g_{33} = r^2 = y^2 + z^2$$

$$J = x_\xi r_\eta - x_\eta r_\xi$$

$$g_{12} = x_\xi x_\eta + r_\xi r_\eta$$

$$g_{13} = g_{23} = 0$$

$$g = r^2[g_{11}g_{22} - (g_{12})^2] = r^2J^2$$

$$g^{11} = r^2 g_{22}/g$$

$$g^{22} = r^2 g_{11}/g$$

$$g^{33} = 1/r^2$$

$$g^{12} = -r^2 g_{12}/g$$

$$g^{13} = g^{23} = 0$$

$$\Gamma^1_{11} = \frac{r^2}{2g}\left[g_{22}\frac{\partial g_{11}}{\partial \xi} - g_{12}\left(2\frac{\partial g_{12}}{\partial \xi} - \frac{\partial g_{11}}{\partial \eta}\right)\right]$$

$$\Gamma^1_{12} = \frac{r^2}{2g}\left[g_{22}\frac{\partial g_{11}}{\partial \eta} - g_{12}\frac{\partial g_{22}}{\partial \xi}\right]$$

$$\Gamma^1_{13} = \Gamma^1_{23} = 0$$

$$\Gamma^1_{22} = \frac{r^2}{2g}\left[g_{22}\left(2\frac{\partial g_{12}}{\partial \eta} - \frac{\partial g_{22}}{\partial \xi}\right) - g_{12}\frac{\partial g_{22}}{\partial \eta}\right]$$

$$\Gamma^1_{33} = \frac{r^3}{g}\left(g_{12}r_\eta - g_{22}r_\xi\right)$$

$$\Gamma^2_{11} = \frac{r^2}{2g}\left[g_{11}\left(2\frac{\partial g_{12}}{\partial \xi} - \frac{\partial g_{11}}{\partial \eta}\right) - g_{12}\frac{\partial g_{11}}{\partial \xi}\right]$$

$$\Gamma^2_{22} = \frac{r^2}{2g}\left[g_{11}\frac{\partial g_{22}}{\partial \eta} - g_{12}\left(2\frac{\partial g_{12}}{\partial \eta} - \frac{\partial g_{22}}{\partial \xi}\right)\right]$$

$$\Gamma^2_{12} = \frac{r^2}{2g}\left(g_{11}\frac{\partial g_{22}}{\partial \xi} - g_{12}\frac{\partial g_{11}}{\partial \eta}\right)$$

$$\Gamma^2_{13} = \Gamma^2_{23} = 0$$

$$\Gamma^2_{33} = \frac{r^3}{g}\left(g_{12}r_\xi - g_{11}r_\eta\right)$$

$$\Gamma^3_{11} = \Gamma^3_{22} = \Gamma^3_{12} = \Gamma^3_{33} = 0$$

$$\Gamma^3_{13} = \frac{r_\xi}{r}$$

$$r_{23}^3 = \frac{r_\eta}{r} \tag{2.15}$$

The base vectors a_i are

$$\begin{aligned} \underset{\sim}{a}_1 &= \underset{\sim}{i}x_\xi + \underset{\sim}{j}r_\xi\cos\phi + \underset{\sim}{k}r_\xi\sin\phi \\ \underset{\sim}{a}_2 &= \underset{\sim}{i}x_\eta + \underset{\sim}{j}r_\eta\cos\phi + \underset{\sim}{k}r_\eta\sin\phi \\ \underset{\sim}{a}_3 &= r(\underset{\sim}{k}\cos\phi - \underset{\sim}{j}\sin\phi) \end{aligned} \tag{2.16}$$

where $\underset{\sim}{i}$, $\underset{\sim}{j}$, $\underset{\sim}{k}$ are the unit vectors along the Cartesian coordinates x, y, z, respectively.

The relations between the Cartesian components of the velocity vector denoted as U, V, W and the contravariant components are

$$\begin{aligned} U &= v^1x_\xi + v^2x_\eta \\ V &= \hat{S}\cos\phi - rv^3\sin\phi \\ W &= \hat{S}\sin\phi + rv^3\cos\phi \end{aligned} \tag{2.17}$$

where

$$\begin{aligned} \hat{S} &= v^1r_\xi + v^2r_\eta \\ &= V\cos\phi + W\sin\phi \end{aligned} \tag{2.18}$$

From (2.17), we have

$$v^1 = (Ur_\eta - \hat{S}x_\eta)/\sqrt{g/r^2}$$

$$v^2 = (Sx_\xi - Ur_\xi)/\sqrt{g/r^2}$$

$$v^3 = (W\cos\phi - V\sin\phi)/r \tag{2.19}$$

It must be noted that rv^3 is the velocity of swirl.

The symmetric momentum-stress tensor X^{ik} appearing in Eq. (2.12) and defined in (2.14) is now used to define another tensor XM^{ik} defined below.

$$XM^{11} = X^{11}x_\xi + X^{12}x_\eta$$

$$XM^{12} = X^{12}x_\xi + X^{22}x_\eta$$

$$XM^{13} = X^{13}x_\xi + X^{23}x_\eta$$

$$XM^{21} = (X^{11}r_\xi + X^{12}r_\eta)\cos\phi - rX^{13}\sin\phi$$

$$XM^{22} = (X^{12}r_\xi + X^{22}r_\eta)\cos\phi - rX^{23}\sin\phi$$

$$XM^{23} = (X^{13}r_\xi + X^{23}r_\eta)\cos\phi - rX^{33}\sin\phi$$

$$XM^{31} = (X^{11}r_\xi + X^{12}r_\eta)\sin\phi + rX^{13}\cos\phi$$

$$XM^{32} = (X^{12}r_\xi + X^{22}r_\eta)\sin\phi + rX^{23}\cos\phi$$

$$XM^{33} = (X^{13}r_\xi + X^{23}r_\eta)\sin\phi + rX^{33}\cos\phi \tag{2.20}$$

When Eqs. (2.16), (2.17) and (2.20) are used in Eqs. (2.11) - (2.13), we get the following equations.

$$\frac{\partial\sigma}{\partial t} + \frac{\partial}{\partial\xi}(\sigma v^1) + \frac{\partial}{\partial\eta}(\sigma v^2) + \frac{\partial}{\partial\phi}(\sigma v^3) = 0 \tag{2.21}$$

$$\frac{\partial}{\partial t}(\sigma U) + \frac{\partial}{\partial \xi}(XM^{11}) + \frac{\partial}{\partial \eta}(XM^{12}) + \frac{\partial}{\partial \phi}(\sigma v^3 U)$$

$$- \varepsilon\left[\frac{\partial}{\partial \xi}\{\lambda(r\frac{\partial v^3}{\partial \phi} + \hat{S})r_\eta\} - \frac{\partial}{\partial \eta}\{\lambda(r\frac{\partial v^3}{\partial \phi} + \hat{S})r_\xi\}\right.$$

$$\left. + \frac{\partial}{\partial \phi}\{\mu r(r_\eta \frac{\partial v^3}{\partial \xi} - r_\xi \frac{\partial v^3}{\partial \eta}) + \frac{\mu J}{r}\frac{\partial U}{\partial \phi}\}\right] = 0 \qquad (2.22)$$

$$\frac{\partial}{\partial t}(\sigma \hat{S}) + \frac{\partial}{\partial \xi}(XM^{21}) + \frac{\partial}{\partial \eta}(XM^{22}) + \frac{\partial}{\partial \phi}(\sigma v^3 U)$$

$$+ \varepsilon\left[\frac{\partial}{\partial \xi}\{\lambda(r\frac{\partial v^3}{\partial \phi} + \hat{S})x_\eta\} - \frac{\partial}{\partial \eta}\{\lambda(r\frac{\partial v^3}{\partial \phi} + \hat{S})x_\xi\}\right.$$

$$\left. - \frac{\partial}{\partial \phi}\{\mu r(x_\xi \frac{\partial v^3}{\partial \eta} - x_\eta \frac{\partial v^3}{\partial \xi}) + \frac{\mu J}{r}(r_\xi \frac{\partial v^1}{\partial \phi} + r_\eta \frac{\partial v^2}{\partial \phi})\}\right]$$

$$- \sigma r(v^3)^2 - P + \varepsilon\chi + \varepsilon J(\lambda + 2\mu)\frac{\partial v^3}{\partial \phi}$$

$$+ \frac{\varepsilon J}{r}(\lambda + 2\mu)\hat{S}$$

$$= 0 \qquad (2.23)$$

$$\frac{\partial}{\partial t}(\sigma v^3) + \frac{1}{r}\frac{\partial}{\partial \xi}(\sigma r v^1 v^3) + \frac{1}{r}\frac{\partial}{\partial \eta}(\sigma r v^2 v^3)$$

$$+ \frac{\partial}{\partial \phi}(\sigma (v^3)^2) - \frac{\varepsilon}{r}\frac{\partial}{\partial \xi}\left[\frac{\mu r^2}{J}(g_{22}\frac{\partial v^3}{\partial \xi} - g_{12}\frac{\partial v^3}{\partial \eta})\right.$$

$$\left. + \mu J\frac{\partial v^1}{\partial \phi}\right] - \frac{\varepsilon}{r}\frac{\partial}{\partial \eta}\left[\frac{\mu r^2}{J}(g_{11}\frac{\partial v^3}{\partial \eta} - g_{12}\frac{\partial v^3}{\partial \xi})\right.$$

$$\left. + \mu J\frac{\partial v^2}{\partial \phi}\right] - \varepsilon\frac{\partial}{\partial \phi}\left[\mu r(x_\xi \frac{\partial v^3}{\partial \eta} - x_\eta \frac{\partial v^3}{\partial \xi})\right.$$

$$\left. + \frac{\mu J}{r}(r_\xi \frac{\partial v^1}{\partial \phi} + r_\eta \frac{\partial v^2}{\partial \phi})\right]$$

$$+ \frac{\sigma}{r} v^3 U - \varepsilon\mu\left(x_\xi \frac{\partial v^3}{\partial \eta} - x_\eta \frac{\partial v^3}{\partial \xi}\right)$$

$$- \frac{\varepsilon\mu J}{r^2}\left(r_\xi \frac{\partial v^1}{\partial \phi} + r_\eta \frac{\partial v^2}{\partial \phi}\right) = 0 \qquad (2.24)$$

$$\frac{\partial E}{\partial t} + \frac{\partial Y^1}{\partial \xi} + \frac{\partial Y^2}{\partial \eta} - \varepsilon\frac{\partial}{\partial \xi}\left[\lambda r J\left(\frac{\partial v^3}{\partial \phi} + \frac{\hat{S}}{r}\right)v^1\right.$$

$$\left. + \mu r J v^3 \frac{\partial v^1}{\partial \phi} + \frac{\mu r^3 v^3}{J}\left(g_{22} \frac{\partial v^3}{\partial \xi} - g_{12} \frac{\partial v^3}{\partial \eta}\right)\right]$$

$$- \varepsilon\frac{\partial}{\partial \eta}\left[\lambda r J\left(\frac{\partial v^3}{\partial \phi} + \frac{\hat{S}}{r}\right)v^2 + \mu r J v^3 \frac{\partial v^2}{\partial \phi}\right)\right]$$

$$\left. + \frac{\mu r^3 v^3}{J}\left(g_{11} \frac{\partial v^3}{\partial \eta} - g_{12} \frac{\partial v^3}{\partial \xi}\right)\right]$$

$$+ \frac{\partial}{\partial \phi}\left[r(E + P)v^3 - \varepsilon\psi^3 - \frac{S\mu J}{r} \frac{\partial R}{\partial \phi}\right] = 0 \qquad (2.25)$$

In numerical vector form, Equations (2.21) - (2.25) can be written as

$$\frac{\partial \underset{\sim}{W}}{\partial t} + \frac{\partial \underset{\sim}{F}}{\partial \xi} + \frac{\partial \underset{\sim}{G}}{\partial \eta} + \frac{\partial \underset{\sim}{E}}{\partial \phi} + \underset{\sim}{H} = 0 \qquad (2.26)$$

For the case of axially symmetric flow at zero angle of attack and with zero swirl the preceding equations become simplified by setting $v^3 = 0$, and $\frac{\partial}{\partial \phi} = 0$

Boundary Conditions:

(i) Free stream conditions:

The flow at upstream infinity is assumed to be uniform at supersonic free stream conditions U_∞^*, ρ_∞^*, p_∞^* at an angle of attack α with the axial direction. The non-dimensional form of the free stream conditions are

$$\rho = 1 \ , \ p = p_\infty \ , \ M = M_\infty$$

$$U = \cos\alpha \ , \ \hat{S} = \sin\alpha\cos\phi \ , \ rv^3 = -\sin\alpha\sin\phi \tag{2.27}$$

(ii) At the body surface:

$$U = \hat{S} = v^3 = 0$$

$$T = T_w \quad \text{or} \quad \left(\frac{\partial T}{\partial n}\right)_w \tag{2.28}$$

(iii) Out-flow plane: zero derivative conditions.

(iv) Symmetry conditions on the planes $\phi = 0$, $\phi = \pi$ for the axially symmetric case.

For the case of aero angle of attack, the calculations on the stagnation line $\xi = \xi_s$ are to be performed separately. Let F be either U, ρ or E. Then on the stagnation line

$$F(\xi_s, \eta, \phi) = F(\xi_s, \eta, \phi+\pi)$$

$$\left(\frac{\partial F}{\partial \xi}\right)_{\substack{\xi=\xi_s \\ \phi=\phi}} = -\left(\frac{\partial F}{\partial \xi}\right)_{\substack{\xi=\xi_s \\ \phi=\phi+\pi}} \tag{2.29}$$

3. NUMERICAL SOLUTION OF THE NAVIER-STOKES EQUATIONS

The numerical methods used to solve the Navier-Stokes equations are presented in this section. The development of finite difference approximations of Equations (2.26) and the algorithm used to solve them are described. Boundary conditions and the calculation of values along the stagnation lines are discussed. The procedures used to control nonlinear instabilities in the solution are described. Finally, a discussion of the initial conditions for the test case used in this research is given.

A. Finite Difference Approximations and the Solution Algorithm

The numerical vector Equation (2.26) for the case of zero angle of attack, $\frac{\partial \tilde{E}}{\partial \phi} = 0$, was discretized into a set of difference equations by replacing the partial derivatives with finite difference approximations. These difference equations were written in a form that allows either of two fully implicit differencing schemes to be used. In both of these schemes, spatial derivatives were replaced by second order central difference approximations. In the first scheme, the time derivative is replaced by a three point backwards difference approximation at N+1 where N is the time step of size Δt.

In the second scheme, the time derivative is replaced by a first order backwards difference at N+1. The spatial derivatives are replaced by the average of the derivatives evaluated at time steps N+1 and N. This scheme is commonly referred to as "trapezoidal" or Crank-Nicolson differencing. Both of these differencing schemes are second order accurate in space and time.

SOR iteration was used to solve the system of equations resulting from the difference approximations described above. The SOR algorithm for both differencing schemes is

$$\underset{\sim}{W}^{N+1}_{I,J} = \underset{\sim}{W}^{N+1(p)}_{I,J} + \omega \underset{\sim}{R}_{I,J} \tag{3.1}$$

where ω is the relaxation parameter and (p) denotes values at the previous iteration. The residual vector, $\underset{\sim}{R}$, is

$$\underset{\sim}{R}_{I,J} = (1+\delta_3)\underset{\sim}{W}^{N}_{I,J} - \delta_3 \underset{\sim}{W}^{N-1}_{I,J} - \underset{\sim}{W}^{N+1(p)}_{I,J} - \delta_2 \Delta t \; RHS^{N+1}_{I,J}$$

$$- (\delta_2 - \delta_3) RHS^{N}_{I,J} \tag{3.2}$$

where

$$RHS_{I,J} = \underset{\sim}{F}_{I+1,J} - \underset{\sim}{F}_{I-1,J} + \underset{\sim}{G}_{I,J+1} - \underset{\sim}{G}_{I,J-1} - 2\underset{\sim}{H}_{I,J} \tag{3.3}$$

In equation (3.2), setting the parameters, $\delta_2 = \delta_3 = 1/3$, yields the three point backwards time differencing scheme. Setting, $\delta_3 = 0$ and $\delta_2 = 1/4$, yields the trapezoidal scheme.

All parameters in Equation (3.2) evaluated at N+1 use the most recent values of $\underset{\sim}{W}$ from the previous iteration. Modifications to Equation (3.2) to control non-linear instabilities are discussed later in this chapter.

B. Boundary Conditions on the Infinity Boundary

The infinity boundary is divided into inflow and outflow regions. The freestream values of the flow variables are maintained along the inflow boundary. Values along the outflow boundary are computed by extrapolation of the physical flow parameters (ρ, U, $\hat{S}$, Ψ) from the field. The extrapolation formulae for the outflow boundary is derived by assuming the spatial derivatives of the flow variables along lines of constant ξ at the outer boundary are equal to zero. The three point backwards difference approximation of the first derivative then can

be used to write the following formula:

$$F_{I,JMAX} = (4F_{I,JMAX-1} - F_{I,JMAX-2})/3 \tag{3.4}$$

where $F = (\rho, U, \hat{S}, \Psi)$ and $J = JMAX$ denotes the outer boundary.

C. Boundary Conditions Along the Body Surface

The body surface is taken to be an impermeable, isothermal boundary. The no slip condition ($U = \hat{S} = v^1 = v^2 = 0$) is imposed along the boundary. Pressure and energy at the boundary are computed by Eqs. (2.5) and (2.9). The wall density is computed by solving the continuity equation at the body surface. The no slip condition permits the continuity equation at the boundary to be written as

$$\left(\frac{\partial \sigma}{\partial t}\right)_{I,1} = - \left(\frac{\partial B}{\partial \eta}\right)_{I,1} \tag{3.5}$$

where $B = \sigma v^2$ and $J = 1$ denotes the body surface.

Two different differencing techniques were used to evaluate Equation (3.5). In the first technique, the time derivative is evaluated at the N+1 time level by a first order backwards difference. The spatial derivative is evaluated at the Nth time level by a three point backwards difference approximation. Equation (3.5) then becomes

$$\sigma^{N+1}_{I,1} = \sigma^{N}_{I,1} - \frac{\Delta t}{6} \{4B^{N}_{I,2} - B^{N}_{I,3}\} \tag{3.6}$$

where $B^{N}_{I,1} = 0$. This equation was used for the first two time steps of the solution. Equation (3.6) is an explicit equation and is known to cause instabilities with repeated use. Therefore, an implicit equation, derived by replacing both the time and the space derivatives with three point backwards differences evaluated at time level N+1, was used at succeeding time steps. These approximations yield

$$\sigma_{I,1}^{N+1} = \frac{1}{3}\left(4\sigma_{I,1}^{N} - \sigma_{I,1}^{N-1}\right) - \frac{\Delta t}{3}\left(4B_{I,2}^{N+1} - B_{I,3}^{N+1}\right) \tag{3.7}$$

where $B_{I,1}^{N+1} = 0$

D. Calculation of Values Along the Stagnation Lines

For axisymmetric flow, Equations (2.26) contain singularities along the forward and rear stagnation lines where r = 0. The values of the flow variables along the stagnation lines must therefore be computed by extrapolation from the field. The extrapolation scheme proposed by Windhopf and Victoria [12] was used in the present research. Let $F(\xi,\eta,\phi)$ be any one of the flow parameters ρ, U, or Ψ on the stagnation lines. Then, by symmetry

$$F(I_s,J,\phi) = F(I_s,J,\phi+\pi) \tag{3.8}$$

and

$$\left(\frac{\partial F}{\partial \xi}\right)_{\phi=\phi} = -\left(\frac{\partial F}{\partial \xi}\right)_{\phi=\phi+\pi} \tag{3.9}$$

where $I_s = I$ at the stagnation line.

An extrapolation formula for the flow variables along the stagnation line can be constructed by replacing the derivatives in Eq. (3.9) by three point forward difference approximations. This substitution and Eq. (3.8) combine to yield

$$F_{I_s,J} = \frac{1}{6}\left[4\left(F_{I_{s+1},J} + F_{I_{s-1},J}\right) - \left(F_{I_{s+2},J} + F_{I_{s-2},J}\right)\right] \tag{3.10}$$

If the symmetry of the flow variables is ideally maintained during the course of the solution, Eq. (3.10) can be replaced by

$$F_{I_s,J} = \frac{1}{3}\left(4F_{I_{s+1},J} - F_{I_{s+2},J}\right) \tag{3.11}$$

Equation (3.11) was initially used to compute the values of the flow variables along the forward stagnation line.

Along the rear stagnation line, the values of the flow variables were computed by averging the values at I=2 and IMAX-1. The Cartesian velocity component, $\hat{S}$, is set to zero along both stagnation lines. The contravariant components of velocity, v^1 and v^2, can then be computed by Equations (2.19). For $\hat{S} = 0$, Eqs. (2.19) yield

$$v^1 = \frac{Ur_\eta}{J} \quad , \quad v^2 = -\frac{Ur_\xi}{J} \tag{3.12}$$

E. Control of Numerical Instabilities

The numerical instabilities described in Chapter 1 are an inherent part of numerical solutions of systems of partial differential equations such as the Navier-Stokes equations. The oscillations in the flow variables that signal the onset of numerical instabilities must be damped as soon as they appear in the solution in order to maintain a stable solution. Although several methods for controlling numerical instabilities have been proposed, the most successful techniques for compressible flow problems have introduced terms into the finite difference approximations of the equations being solved to "filter" or "smooth" the oscillations. These additional terms act to add artificial viscosity that increase the effects of dissipation in the solution. An equivalent method is to add an explicit artificial viscosity term to the calculation of the coefficient of viscosity, μ. Both of these methods were used in the present research.

Initially, the Shuman filtering technique employed by Viegenthart [13] and Harten and Zwas [14] was used. The Shuman filter is implemented by replacing $\underset{\sim}{W}^N$ and $\underset{\sim}{W}^{N-1}$ in Eq. (3.2) with

$$\underset{\sim}{W}_{I,J} + \frac{\bar{\alpha}}{4} \, rJ \, [\underset{\sim}{\bar{W}}_{I+1,J} + \underset{\sim}{\bar{W}}_{I-1,J} + \underset{\sim}{\bar{W}}_{I,J+1} + \underset{\sim}{\bar{W}}_{I,J-1} - 4\underset{\sim}{\bar{W}}_{I,J}] \qquad (3.13)$$

where $\underset{\sim}{\bar{W}}_{I,J}$ represents the physical values of the flow variables $(\rho,\rho U,\rho\hat{S},\Psi)$ and $\bar{\alpha}$ is a switching parameter that can be used to turn the filter on and off or to vary the strength of dissipation. Setting $\bar{\alpha}$ equal to 0.5 yields the form of the Shuman filter used in Refs. [1,2,3]. Application of this form of the filter at all points in the field will eliminate oscillations in the flow variables. However, the excessive dissipation introduced by the full Shuman filter lowers the effective Reynolds number of the flow and delays convergence to a steady state. Therefore, it is desirable to apply the filter only in regions where oscillations occur. This can be accomplished by setting the value of the switching parameter by either of two methods.

In the first method, the field is searched prior to the start of a time step for N shaped wave forms. The filter is then applied at the inner points of the N-wave. The second method is similar to the technique used in Ref. [14]. The value of $\bar{\alpha}$ is varied from point to point in proportion to the magnitude of the local gradient of one of the flow variables such as density or pressure. Therefore, more diffusion will be applied in regions of high gradients, such as across shock waves, where numerical instabilities have a tendency to occur. It should be pointed out that the N-wave and the switched forms of the Shuman filter will not completely eliminate oscillations enough to allow the solution to converge the steady state.

Because of the severity of the full Shuman filter, a second technique for introducing dissipation into the solution was tried. This technique adds an explicit fourth order artificial viscosity term to the computation of the viscosity coefficient. This method of adding artificial viscosity

is related to the fourth order smoother used by Baldwin and MacCormack [15] and was used successfully by Thompson [16] in an incompressible flow problem. In the current research, this method was implemented by replacing the viscosity computed by Sutherland's law with

$$\mu = \mu_s \left[1 + C\left(\frac{\partial^2 P}{\partial \xi^2} + \frac{\partial^2 P}{\partial \eta^2}\right)\right] \tag{3.14}$$

where μ_s is the viscosity given by Eq. (2.6). C is an arbitrary constant whose magnitude is determined experimentally.

F. Initial Conditions

The uniform flow conditions used in this research were as follows: $M_\infty = 22.04$, $|V_\infty^*| = 7000.0$ m/sec, $\rho_\infty^* = 7.73067 \times 10^{-5}$ kg/m^3, and $T_\infty^* = 250.81^\circ$K. From these conditions the pressure, coefficient of viscosity and Knudsen number are computed to be: $P_\infty^* = 5.57043$ N/m^2, $\mu_\infty^* = 1.60209 \times 10^{-5}$ kg/m-sec and $K_{n_\infty} = 0.000193$. For a body diameter of five meters, the free stream Reynolds number is equal to 168888. The ratio of specific heats was assumed to be $\gamma = 1.41$. An isothermal wall temperature, $T_w^* = 1000.0^\circ$K, was maintained throughout the course of this research.

Because the solution algorithm used in the present investigation is iterative, an initial guess for the values of the flow variables is needed at all field points in order to start the solution. However, finding a method of starting the solution that didn't diverge in the initial time step proved to be one of the major tasks of this research project. Although several methods of starting the solution were attempted, only one technique provided an initial guess that would converge for the first time step. In this technique, the U component of velocity is assumed to vary linearly along a line of constant ξ

from the body to the outer boundary. The $\hat{S}$ component of velocity was assumed to be zero. Temperature, pressure and density at all points in the field was assumed to be equal to their values along the outer boundary. A similar technique was applied in Refs. [8,9,10] to initialize the values of the flow variables in the region between the body and the bow shock wave. In the present research, it was found that this method would converge if the time step size was lowered to $\Delta t = .001$. The acceleration parameter was 0.9 for all four equations of motion. Although the first time step converged using this method of starting, the full Shuman filter was required for about ten time steps to maintain stability

4. COMPUTATIONAL PROCEDURES AND RESULTS

A. Computational Procedures

The numerical techniques described in the previous chapter were used to write a computer program that can solve the Navier-Stokes equations for either 2D or axisymmetric flow about an arbitrary axially-symmetric blunt body. The solution process begins with the generation of a coordinate system and the calculation of the corresponding metric data for a prescribed body and an outer boundary cf. Fig. 2. As shown in Fig. 3, the outer boundary used in the present research is an ellipse centered at the midpoint of the body. It is assumed that the outer boundary is placed far enough away from the body surface so that the flow on the downstream boundary will be supersonic. The region between the sixth and the forty-sixth lines of constant ξ is taken as the outflow boundary.

Once the metric data for a given coordinate system is computed and stored on file, the actual solution of the Navier-Stokes equations is begun by assuming an initial guess of the solution for the entire computational domain. The solution is then advanced through time until a steady state solution is reached. However, as has been previously mentioned, finding an initial guess that did not diverge in the first time step proved to be one of the major tasks of this research.

It was originally intended to first obtain a steady state solution for the case of 2D flow and then use the resulting data as an initial guess for the axisymmetric flow case. Generally, the uniform flow conditions along the upstream boundary can be used to provide an initial value at each field point since the initial guess and the resulting transient solution are not required to be physically realistic. For this initial guess, the boundary conditions along the

wall become the driving functions for the solution. However, as in Ref. [3], it was found that this method would not work when the free stream Mach number is very high. After considerable numerical experimentation, it was found that the solution could be started at the desired Mach number (22.04) by assuming a linear variation in velocity between the body and outer boundary along lines of constant ξ. Energy and density were set to the free stream values at all points in the field. However, this technique had two disadvantages. The first disadvantage was that the time step size had to be lowered to .001 for a fixed acceleration parameter of 0.9 for all the four equations of motion. Extensive numerical experimentation did not produce a combination of time step and acceleration parameter that would allow a larger time step to be used. The second disadvantage was that the values of temperature, velocity, and pressure in the region between the expected location of the bow shock and the outer boundary produced by the linear velocity distribution differed substantially from the free stream values. The formation of a shock transition region was therefore substantially delayed because of the time required for the free stream flow to convect into this region and increase the magnitude of the velocity toward the free stream value at a time step of .001. The 2D case was started using the linear velocity distribution and run for several hundred time steps. Although the solution showed signs of eventually approaching the free stream in the region in front of the shock, the computer time required to obtain a steady state solution would have been considerable.

Figures 4 and 5 present distributions of temperature and velocity magnitude along the stagnation line that are typical of the linear velocity distribution initial guess.

At this point in time, the cost of using the local computing facility became prohibitive. Further progress was delayed until arrangements could be made to use the computational facilities at NASA's Marshall Space Flight Center. Because of the delay induced by the transfer of the computer program to NASA-Marshall and the time limits imposed by contractual requirements, it was decided to abandon attempts to obtain a steady state 2D solution. Instead, the methods described above were used to restart the solution for the case of axisymmetric flow. In an attempt to speed up the solution process, a transition region between the values of the flow variables at the anticipated location of the bow shock and the free stream values was introduced explicitly after fifty time steps. The stand off distance of the shock along the stagnation line was computed using the empirical equations of Billig [17]. A linear variation between the values of the flow variables at the η location directly in front of the anticipated shock location and the free stream values was taken over five cell lengths in the η direction. The solution was continued in a normal manner from this point on.

It was found that the full Shuman filter described in the previous chapter was required to control instabilities induced in solving the finite difference equations. However, once the flow field was established, it was found that repetitive use of the full Shuman filter tended to smear the shock transition region toward the outer boundary. Unfortunately, the dissipation introduced by the full filter was required to control the "wiggles" that appeared in the flow variables. The switched and N-wave forms of the filter did not appear to introduce enough dissipation to control these oscillations.

At this point, the calculation of the explicit artificial viscosity

term described in the previous chapter was introduced into the program. It was found that the arbitrary constant, C, had to be on the order of 10^{-6} for the method to be effective. This method of introducing dissipation seemed to work quite well at first. However, as the solution progressed in time, the value of the temperature along the stagnation line in the region where the shock wave had started to form suddenly started to decrease. This trend continued until a negative value of temperature was reached. It is felt that modifying the viscosity coefficient in this manner produced unrealistic values of energy that lead to the calculation of the negative temperature.

The solution has been run through 700 time steps at a step size of 0.001. Efforts to increase this step size have been unsuccessful. For a fixed acceleration parameter of 0.9, it took on the average .825 min. of computer time to converge a time step to a tolerance of 10^{-5}. Convergence was usually obtained after two or three iterations. For a 51 × 50 mesh, this time represents a computational effort of about .0194 sec. per grid point per time step.

All runs were made on UNIVAC 1100/80 series computers at Mississippi State University and NASA-Marshall. The computer program was written in FORTRAN using the UNIVAC ASCII FORTRAN compiler. This program required approximately 102,000 words of core on the 1100/80.

B. Discussion of Results

The solution of the Navier-Stokes equations for the case of axisymmetric flow with the initial conditions given in the previous chapter has been obtained through a non-dimensional time of 0.7. Since this is still a very early time, the results at this time can only be considered as preliminary. Therefore, only qualitative

judgments can be made about the following results. Figures 6-11 depicts the non-dimensional values of density pressure, temperature, and velocity magnitude along the forward stagnation line (I = 26) at a non-dimensional time of 0.7. The trends in these values seem satisfactory. The transition region that denotes the existence of the shock wave is readily seen. The standoff distance of the shock as given by the plots of temperature and pressure compare favorably with the standoff distance computed by the empirical equations given in Ref. [17]. Density and velocity magnitude are plotted as functions of both the non-dimensional distance from the nose of the body and the coordinate η. The pronounced rise in density in the viscous region close to the body is clearly seen in Figures 6 and 7.

Figures 8 and 9 show that the velocity profile in the transition region has been smeared over about twelve grid cells. The temperature profile along the stagnation line is given in Figure 10. The maximum value of temperature shown in the plot seems unrealistically high. This is thought to be due to a combination of the transient nature of the flow and the assumption of an ideal gas. Figure 11 presents the distribution of pressure along the stagnation line. Figure 12 represents a plot of density contours about the body whose values are greater than that of free stream values. This plot indicates a large region of rarefied flow extending over much of the field. This rarefaction is felt to be a transient phenomena induced by the initial guess.

5. CONCLUSIONS AND RECOMMENDATIONS

A method for solving the Navier-Stokes equation for hypersonic flow about axially symmetric bodies has been presented. Although only preliminary results have been obtained, the following conclusions can be drawn.

(1) The technique offers significant computational advantages because of the conservation law form of the equations and the reduced amount of metric data required for axisymmetric and 3D flow calculations.

(2) The major difficulty encountered with the method was finding an initial guess that would remain stable and converge to a realistic solution. Although the linear velocity variation technique used in the present research supplied a stable initial solution, large amounts of dissipation were required to maintain stability. The time step imposed by this starting method also is very costly in terms of computer time. The method of starting from a steady state 2D solution needs to be pursued. A gradual start in which the solution is started at a lower Mach number and gradually brought up to the desired Mach number should be investigated.

(3) The problem of controlling numerical instabilities was not satisfactorily reconciled. Although the switched form of the Shuman filter was not particularly effective in this research, it seems to offer the most promise for reducing the severity of numerical instabilities without substantially retarding the progress of the flow toward steady state.

(4) A more refined mesh system should be employed to increase the accuracy of the solution in the region of the bow shock.

REFERENCES

1. Warsi, Z. U. A., Devarayalu, K., and Thompson, J. F., "Numerical Solution of the Navier-Stokes Equations for Arbitrary Blunt Bodies in Supersonic Flows," Numerical Heat Transfer, Vol. 1, 1978, p. 499.

2. Warsi, Z. U. A., Devarayalu, K., and Thompson, J. F., "Numerical Solution of the Navier-Stokes Equations for Blunt Nosed Bodies in Supersonic Flows," Report MSSU-EIRS-ASE-78-1, Engineering and Industrial Research Station, Mississippi State University (1978).

3. Devarayalu, K., "Numerical Solution of the Navier-Stokes Equations for Supersonic Flows with Strong Shocks," Ph.D. Dissertation, Mississippi State University (1978).

4. Thompson, J. F., Thames, F. C., and Mastin, C. W., "Automatic Numerical Generation of Body Fitted Curvilinear Coordinate System for Field Containing any Number of Arbitrary Two-Dimensional Bodies," Journal of Computational Physics, Vol. 15, 1974, p. 299.

5. Warsi, Z. U. A., and Thompson, J. F., "Machine Solutions of Partial Differential Equations in the Numerically Generated Coordinate Systems," Report MSSU-EIRS-ASE-77-1, Engineering and Industrial Research Station, Mississippi State University (1976).

6. Thompson, J. F., "Numerical Solution of Flow Problems Using Body-Fitted Coordinate Systems," Lecture Series in Computational Fluid Dynamics, von Karman Inst. for Fluid Dynamics, Belgium (1978).

7. Warsi, Z. U. A., "Conservation Form of the Navier-Stokes Equations in General Non-Steady Coordinate Systems," to appear in AIAA Journal.

8. Tannehill, J. C., Holst, T. L., and Rakich, J. V., "Numerical Computation of Two-Dimensional Viscous Blunt Body Flows with an Impinging Shock," AIAA Journal, Vol. 14, No. 2, 1976, p. 204.

9. Rakich, J. V., Vigneron, Y. G., Tannehill, J. C., "Navier-Stokes Calculations for Laminar and Turbulent Hypersonic Flow Over Indented Nosetips," AIAA Paper 78-260, Huntsville, Alabama, 1978.

10. Kutler, P., Chakravarthy, S. R., Lombard, C. K., "Supersonic Flow over Ablated Nosetips Using an Unsteady Implicit Numerical Procedure," AIAA Paper 78-213, Huntsville, Alabama, 1978.

11. Weed, R. A., "Numerical Solution of the Navier-Stokes Equations for Hypersonic Flow about Axially-Symmetric Blunt Bodies," M.S. Thesis, Mississippi State University, August 1980.

12. Widhopf, G. F. and Victoria, K. J., "On the Solution of the Unsteady Navier-Stokes Equations Including Multicomponent Finite Rate Chemistry," Computers and Fluids, Vol. 1, 1973, p. 159.

13. Vliegenthart, A. C., "The Shuman Filtering Operation and the Numerical Computation of Shock Waves," Journal of Engineering Math, Vol. 4, No. 4, 1970, p. 341.

14. Harten, A. and Zwas, G., "Switched Numerical Shuman Filters for Shock Calculations," Journal of Engineering Math, Vol. 6, No. 2, 1972, p. 207.

15. Baldwin, B. S. and MacCormack, R. W., "Interaction of Strong Shock Wave with Turbulent Boundary Layer," AIAA Paper 74-558, Palo Alto, California, June 1974.

16. Thompson, D. S., "Numerical Solution of the Navier-Stokes Equations for High Reynolds Number Incompressible Turbulent Flow," M.S. Thesis, Mississippi State University (1980).

17. Billig, F. S., "Shock-Wave Shapes Around Spherical and Cylinderical-Nosed Bodies," J. Spacecraft, Vol. 1, No. 6, 1967, p. 822.

18. Zucrow, M. J. and Hoffman, J. D., "Gas Dynamics," John Wiley and Sons, 1976.

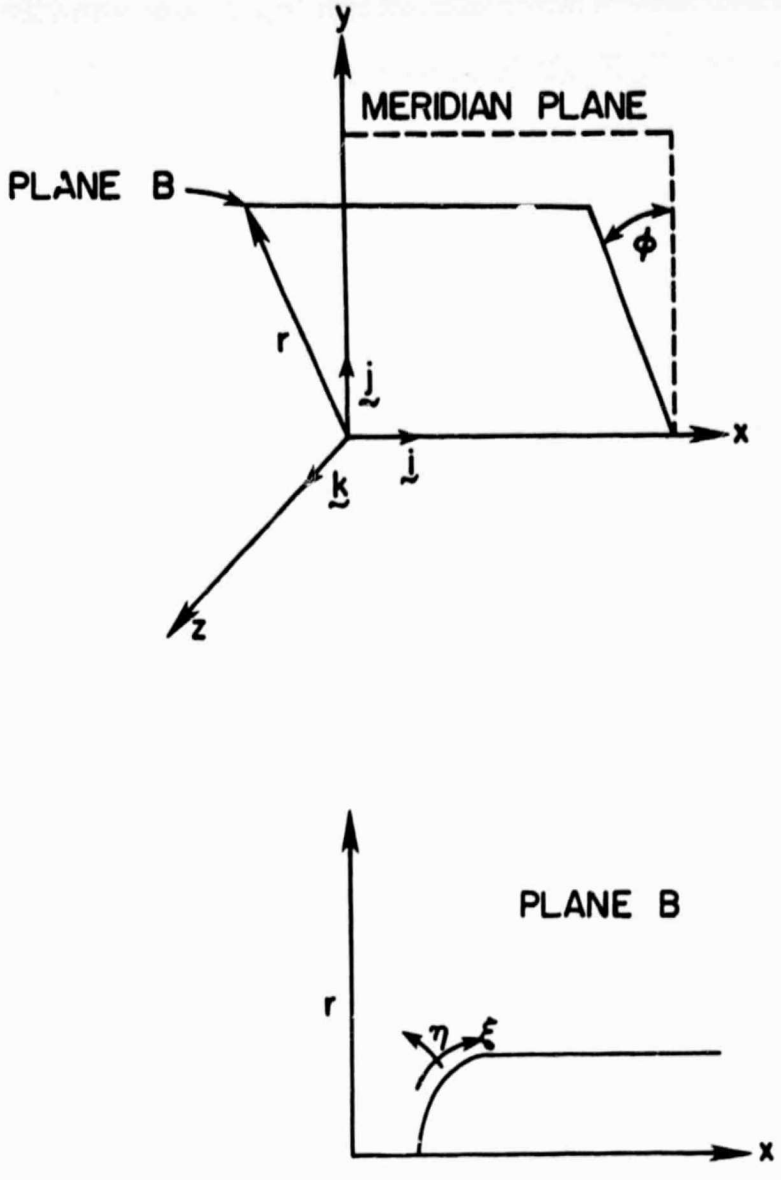

Figure 1. Coordinate Systems Used in Definition of Metric Data

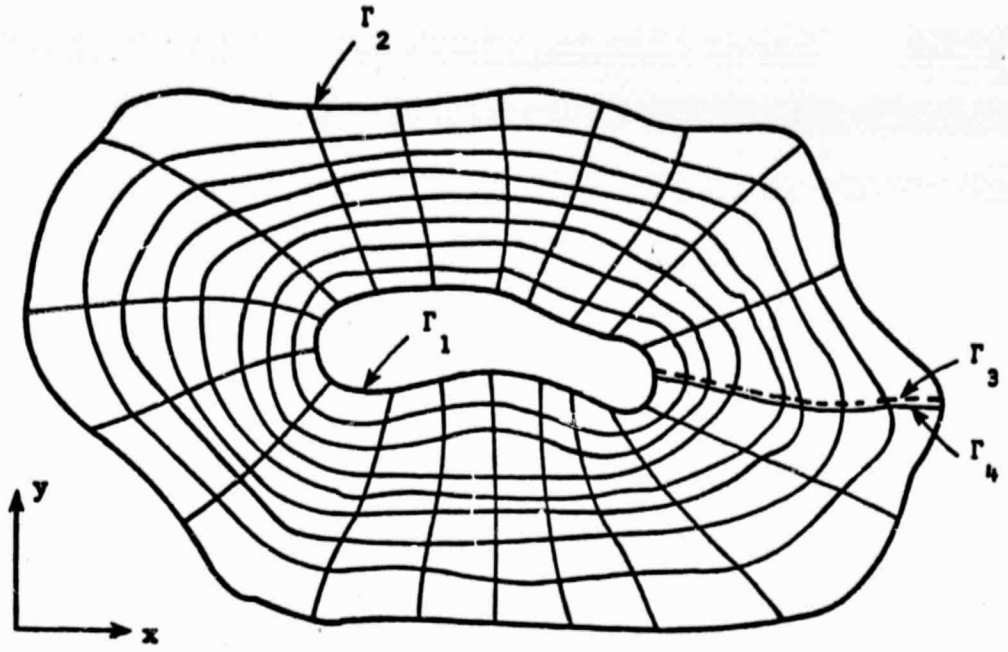

Figure 1. Physical Plane.

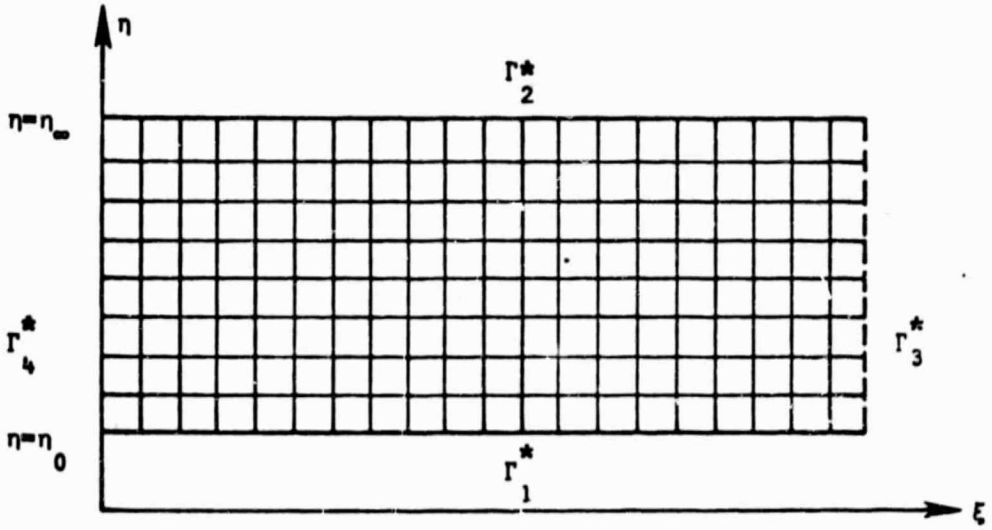

Transformed Plane
(Natural Coordinates)

Figure 2. Field Transformation.

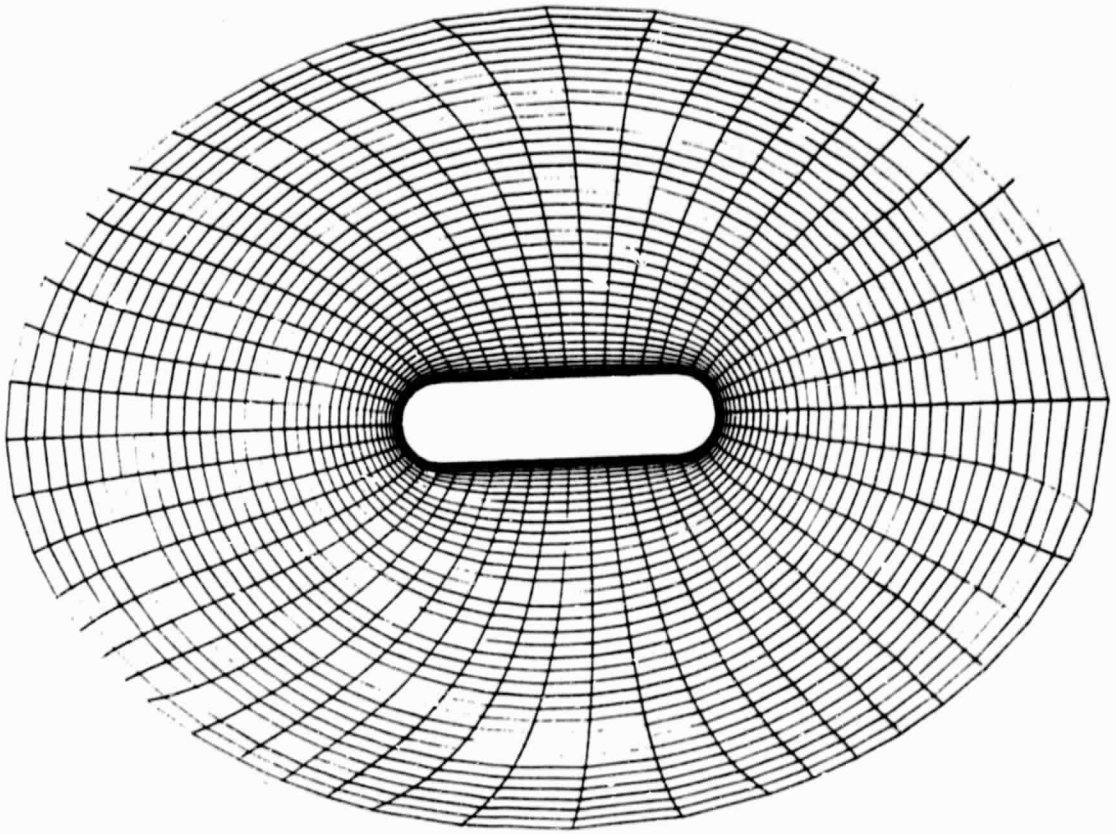

Figure 3. The Computational Coordinate System

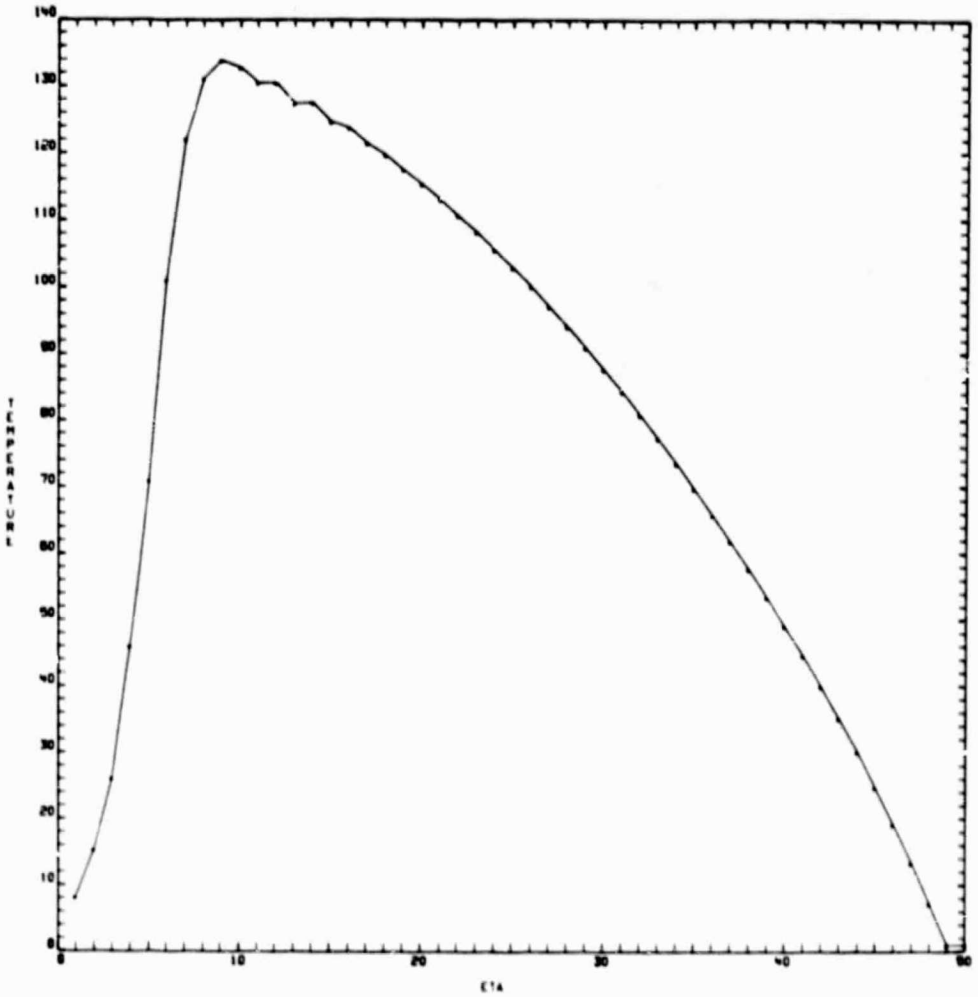

Figure 4. Temperature Distribution Along the Stagnation Line at Time 0.05.

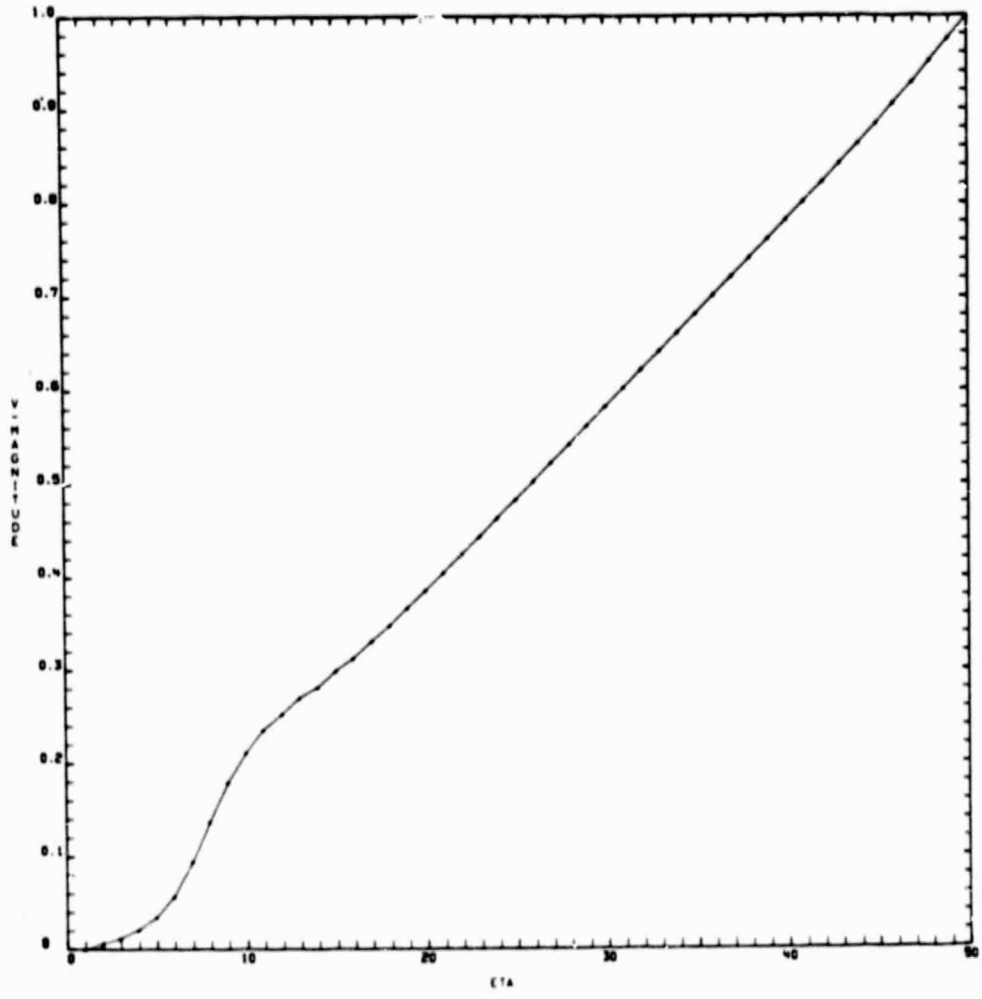

Figure 5. Velocity Distribution Along the Stagnation Line at Time 0.05.

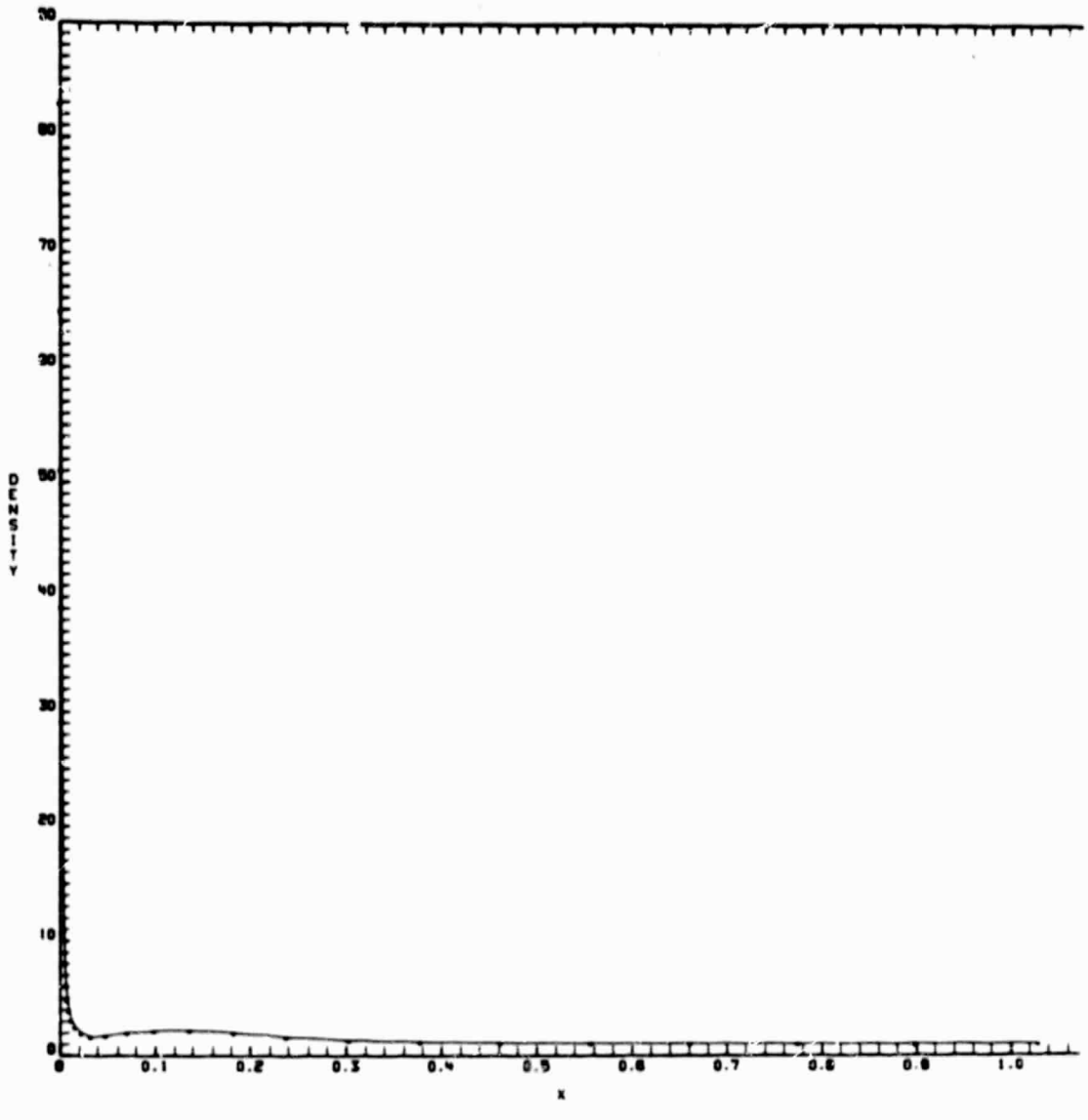

Figure 6. Density Distribution Along the Stagnation Line at Time 0.7.

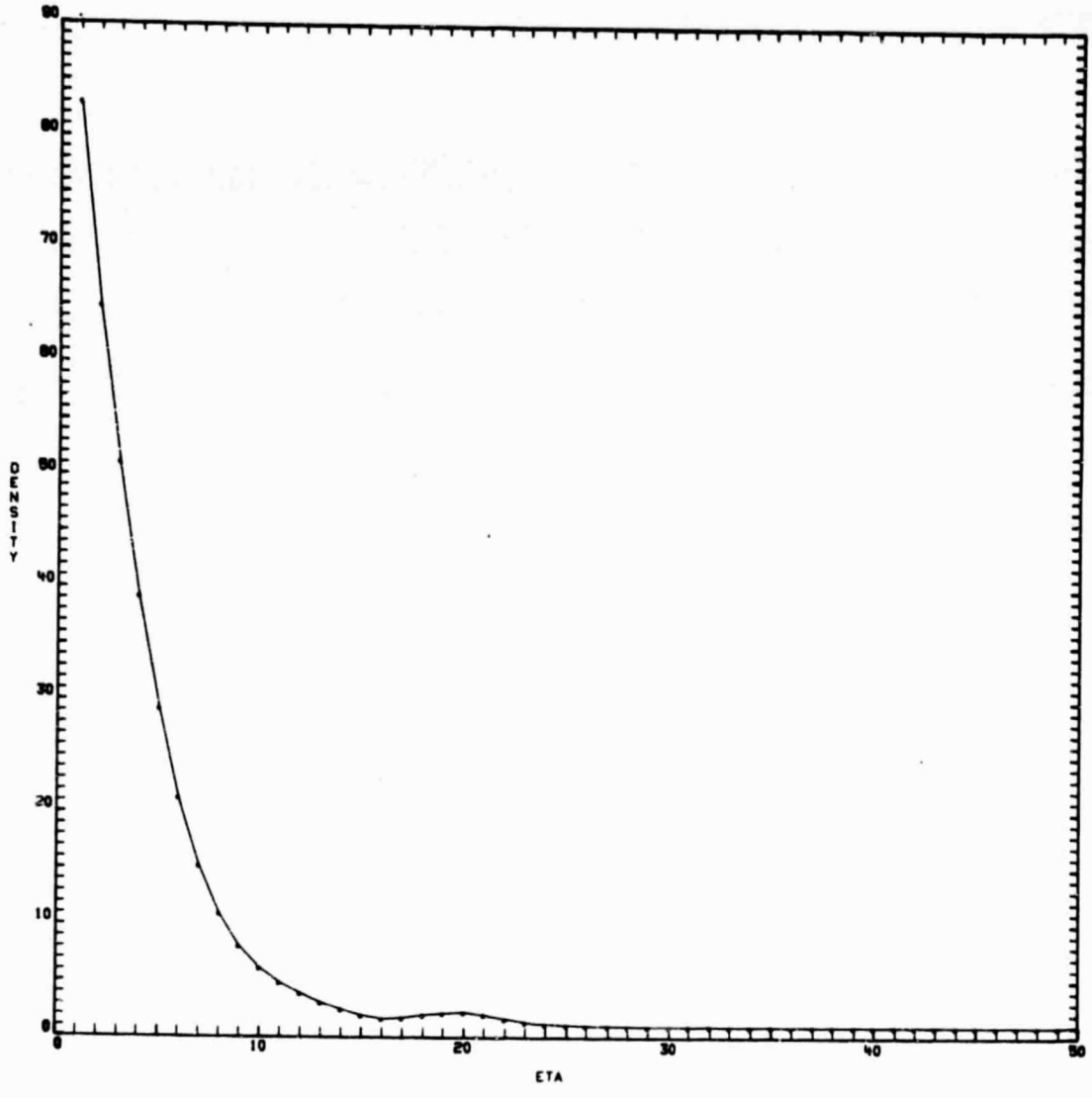

Figure 7. Density Distribution Along the Stagnation Line as a Function of η at Time 0.7.

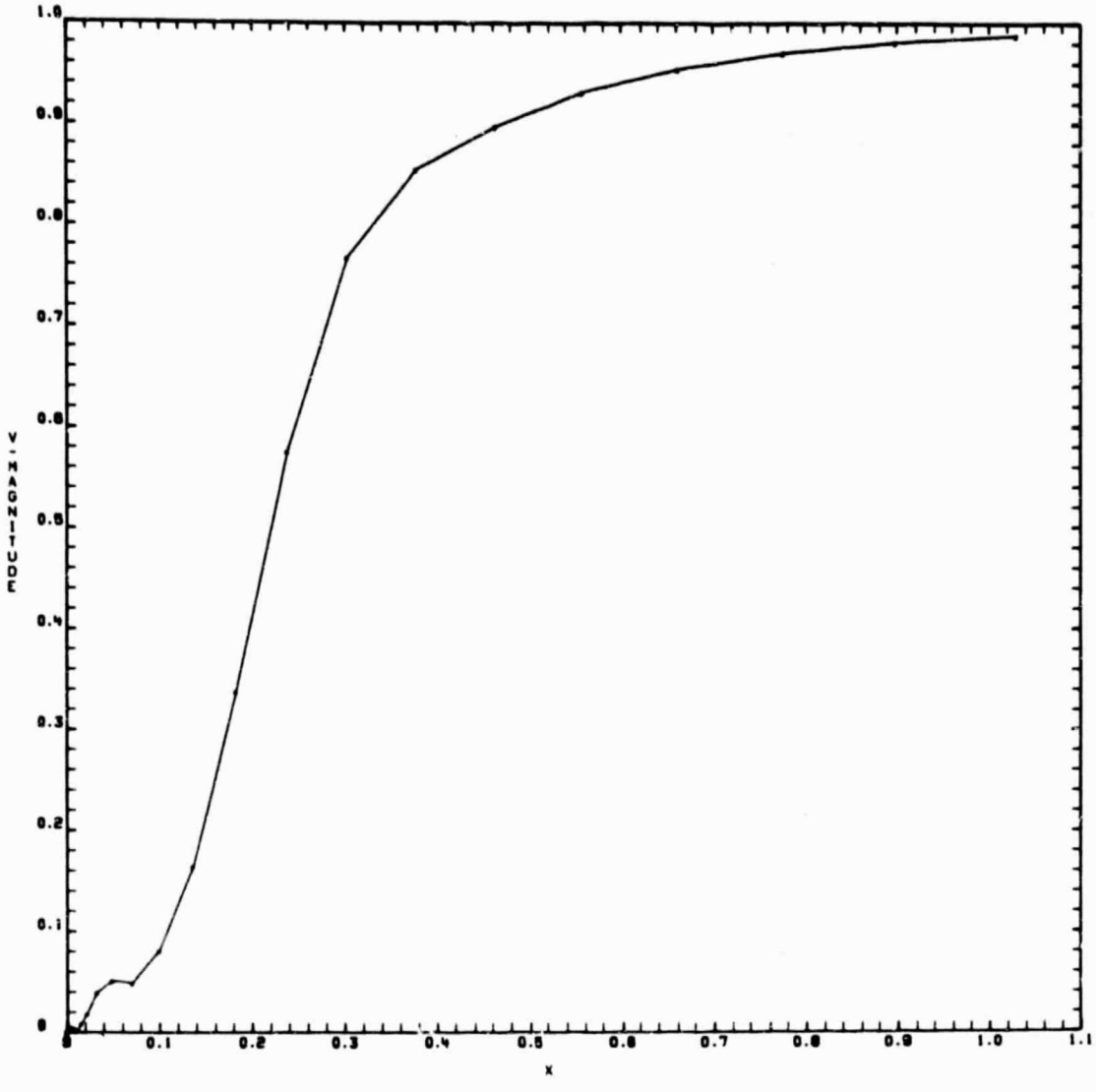

Figure 8. Velocity Distribution Along the Stagnation Line at Time 0.7.

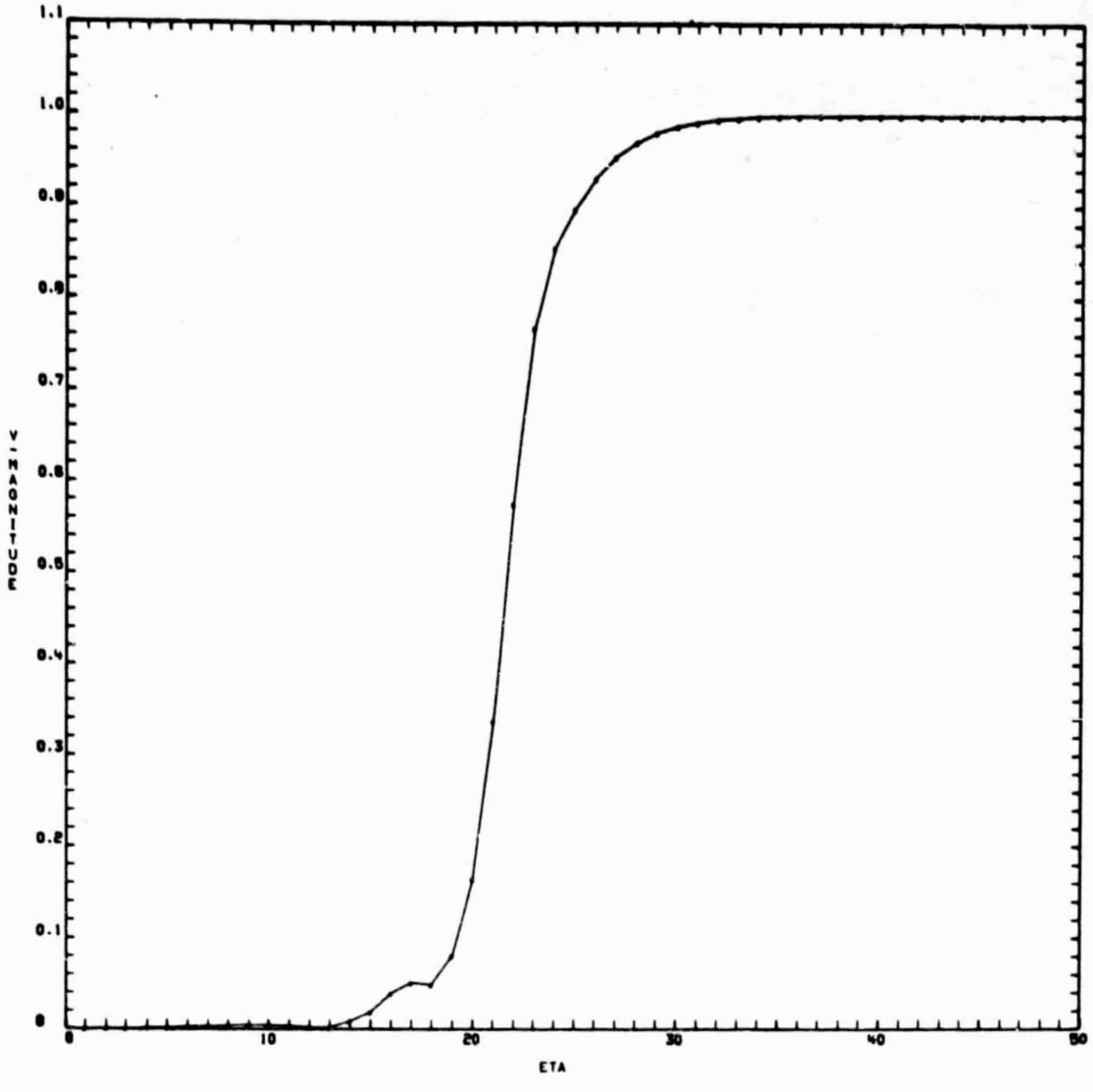

Figure 9. Velocity Distribution Along the Stagnation Line at a Function of η at Time 0.7.

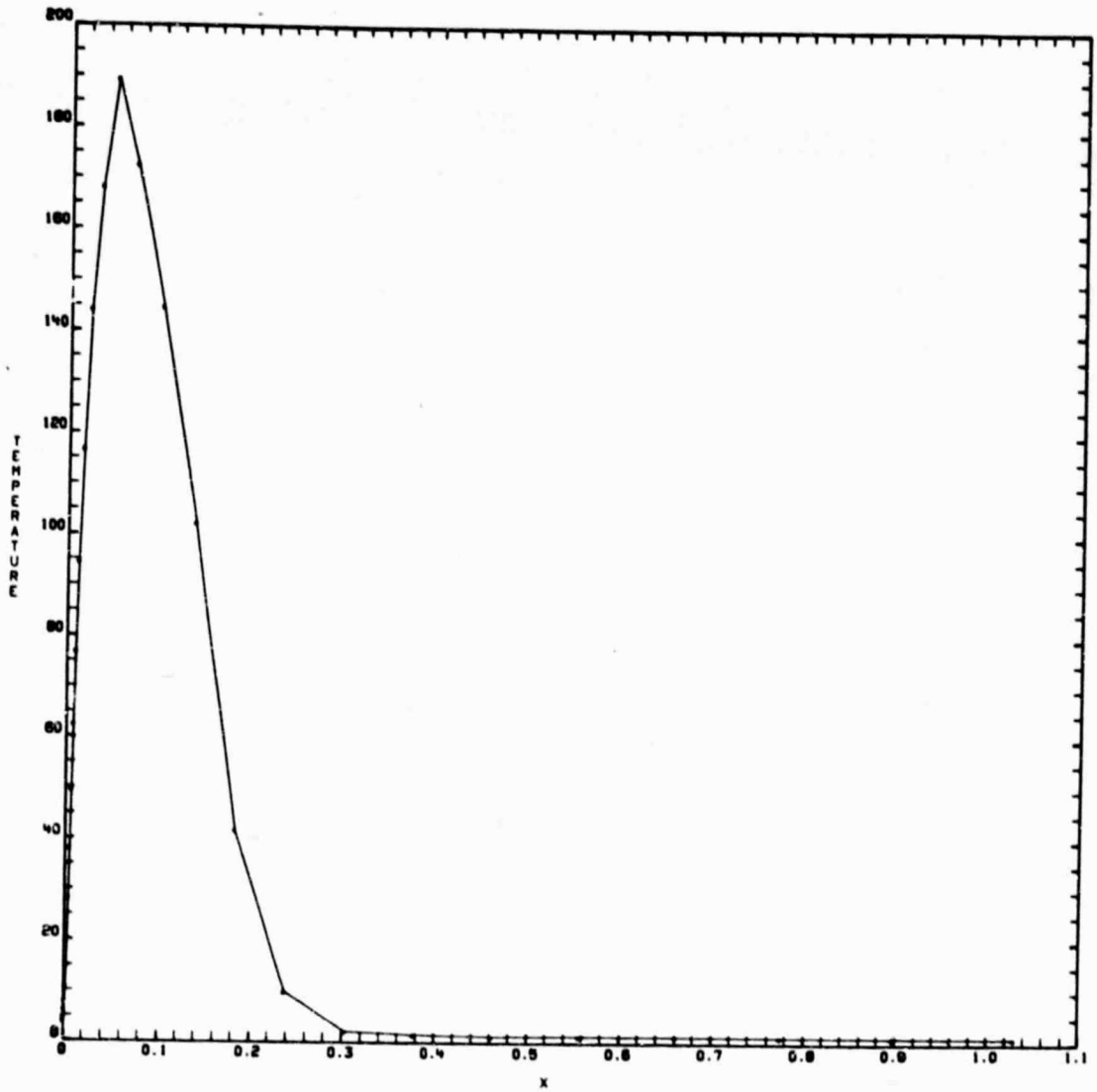

Figure 10. Temperature Distribution Along the Stagnation Line at Time 0.7.

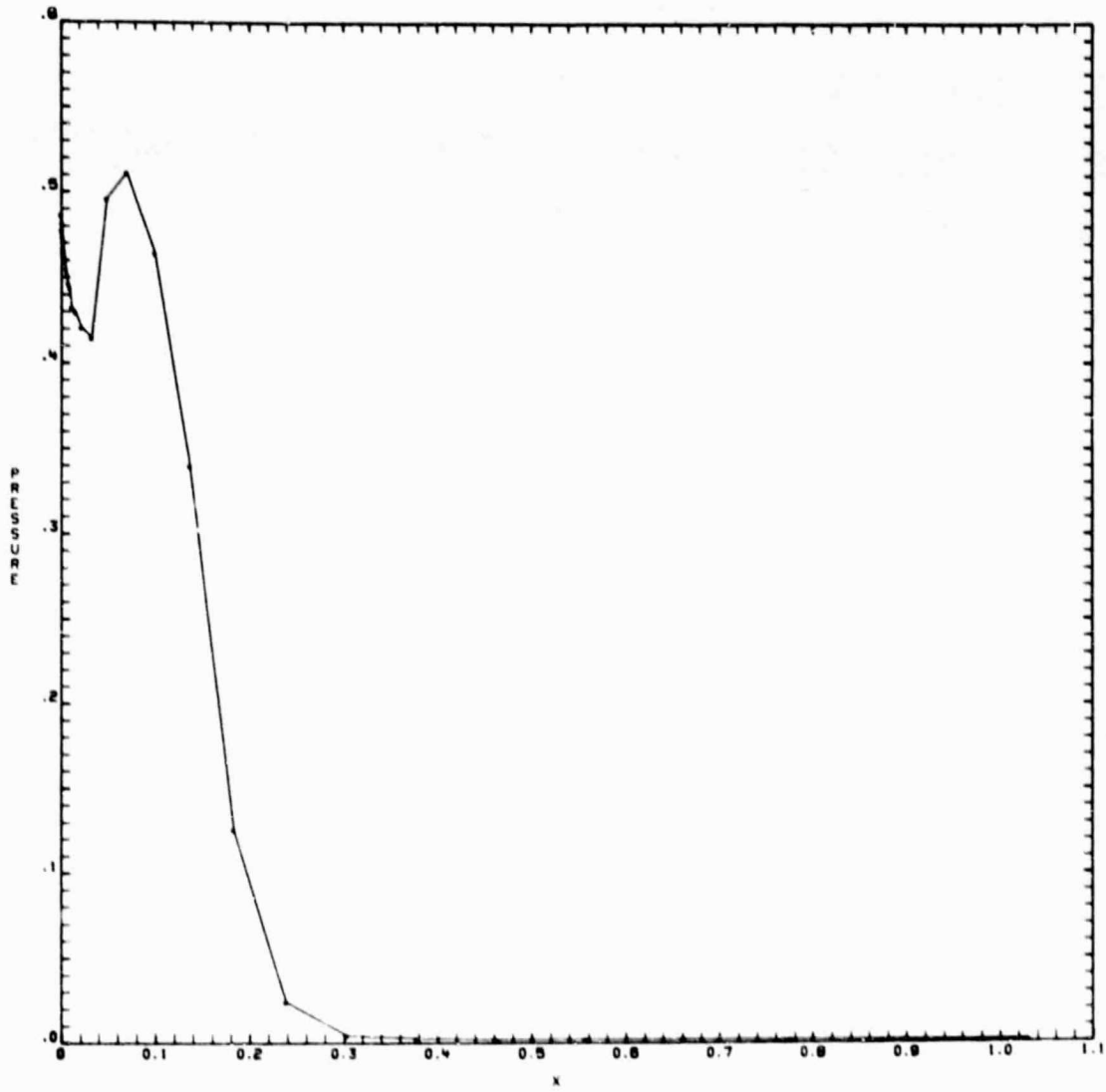

Figure 11. Pressure Distribution Along the Stagnation Line at Time 0.7.

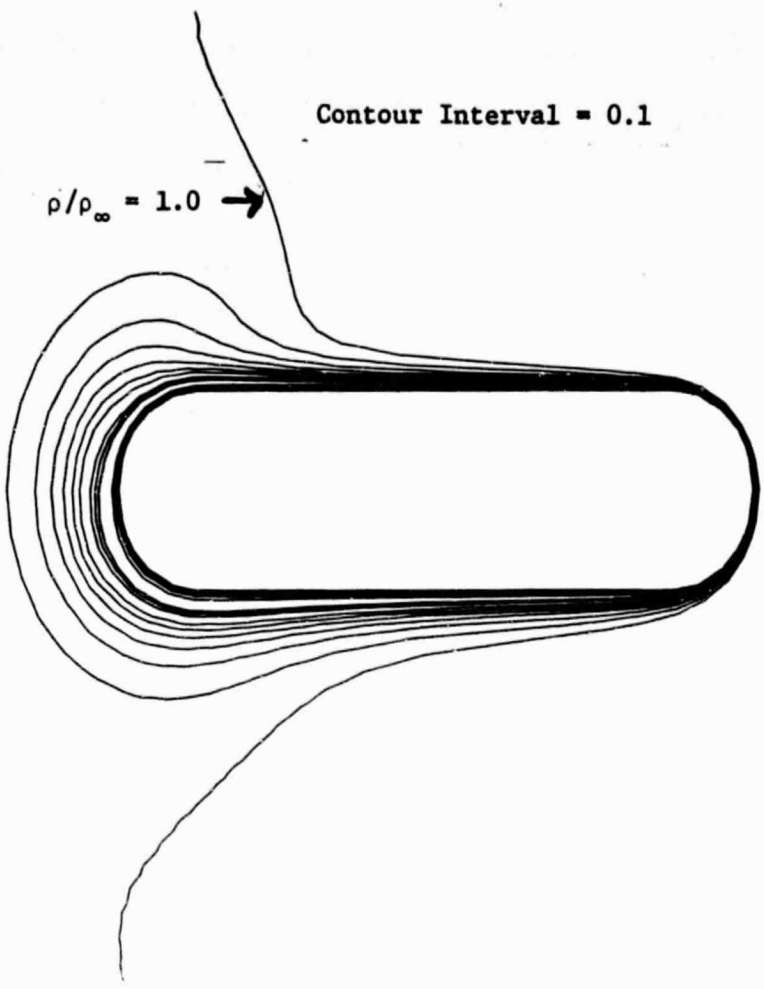

Figure 12. Density Contours at Time 0.7.

Appendix

Thermodynamic Equations

On the molal basis, the specific heat at constant pressure of a thermally perfect gas in the range 300°K to 1000°K is given by, [18],

$$\bar{C}_p^* = \bar{R}(A_1 + A_2 T^* + A_3 T^{*2} + A_4 T^{*3} + A_5 T^{*4}) \ , \tag{A-1}$$

where the constant A_i have been given after Eq. (2.10), and $\bar{R}$ is the universal gas constant,

$$R = 8314.3 \text{J/kgmol} - °\text{K} \ .$$

Introducing

$$C_p^* = \frac{\bar{C}_p^*}{\bar{m}} \ , \quad R = \frac{\bar{R}}{\bar{m}}$$

where $\bar{m}$ is the molecular weight, we have

$$C_p^* = R(A_1 + A_2 T^* + A_3 T^{*2} + A_4 T^{*3} + A_5 T^{*4}) \tag{A-2}$$

On non-dimensionalization

$$T = \frac{T^*}{T_\infty^*} \ , \quad C_p = \frac{C_p^*}{C_{p\infty}^*}$$

we obtain

$$C_p = \frac{f(T)}{f(1)} \tag{A-3}$$

where f(T) has been defined in Eq. (2.10).

Note that

$$C^*_{p\infty} = Rf(1) \tag{A-4}$$

The ratio of the specific heats C^*_p and C^*_v denoted as

$$\gamma = C^*_p/C^*_v$$

can now be expressed a function of T by using the thermodynamic equation

$$C^*_p - C^*_v = R$$

and the Eqs. (A-3) and (A-4) as

$$\gamma(T) = \frac{f(T)}{f(T) - 1} \tag{A-5}$$

For a thermally perfect gas

$$de^* = C^*_v dT^* \tag{A-6}$$

and

$$dh^* = C^*_p dT^* \ . \tag{A-7}$$

On non-dimensionalization, Eq. (A-6) becomes

$$de = \frac{T^*_\infty C^*_{p\infty}}{U^{*2}_\infty} \frac{C_p}{\gamma} dT \tag{A-8}$$

Using (A-3), (A-4) and (A-5), we get

$$de = C_2[f(T) - 1]dT$$

where,

$$C_2 = C_1/f(1)$$

$$C_1 = \frac{RT_\infty^*}{U_\infty^{*2}} f(1) \tag{A-9}$$

Substituting (2.10) for f(T) in Eq. (A-8) and integrating, we obtain

$$e(T) = C_2[(A_1 - 1)T + \frac{1}{2}(A_2T_\infty^*)T^2 + \frac{1}{3}(A_3T_\infty^{*2})T^3$$

$$+ \frac{1}{4}(A_4T_\infty^{*3})T^4 + \frac{1}{5}(A_5T_\infty^{*4})T^5] \tag{A-10}$$

Having expressed e as a function of T, we now use the expression for e from (2.4) to have

$$e = \frac{\Psi}{\rho} - \frac{1}{2}|\underset{\sim}{v}|^2 \tag{A-11}$$

Substituting e(T) from (A-10) in (A-11) we get a fifth degree equation for obtaining the temperature, viz., Equation (2.9).